Volume 14
Number 16
21 August 2024
Pages 4379–4728

# Catalysis Science & Technology

rsc.li/catalysis

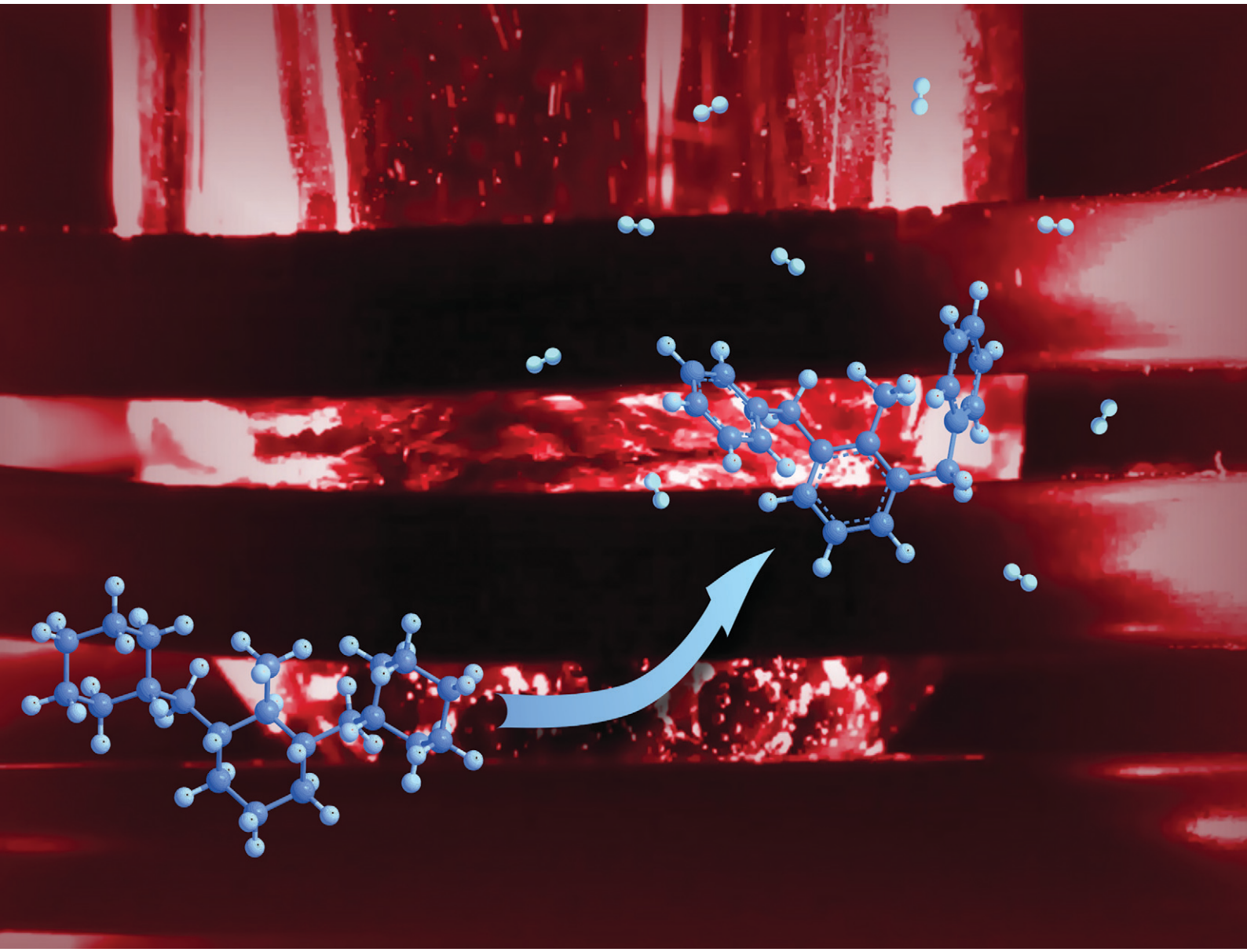

ISSN 2044-4761

ROYAL SOCIETY OF CHEMISTRY

**COMMUNICATION**

Susanne Wintzheimer, Patrick Schühle *et al.*
Inductively heatable catalytic materials for the dehydrogenation of the liquid organic hydrogen carrier (LOHC) perhydro dibenzyltoluene

Catalysis Science & Technology

ROYAL SOCIETY OF CHEMISTRY

COMMUNICATION

View Article Online
View Journal | View Issue

Check for updates

Cite this: *Catal. Sci. Technol.*, 2024, **14**, 4450

Received 28th February 2024,
Accepted 12th July 2024

DOI: 10.1039/d4cy00272e

rsc.li/catalysis

Open Access Article. Published on 19 July 2024. Downloaded on 8/10/2025 9:45:46 PM.
This article is licensed under a Creative Commons Attribution 3.0 Unported Licence.

# Inductively heatable catalytic materials for the dehydrogenation of the liquid organic hydrogen carrier (LOHC) perhydro dibenzyltoluene†

Markus Schörner,‡[a] Thomas Solymosi,‡[a] Theodor Razcka,[b] Phillip Nathrath,[c] Nicolas Patrick Johner,[a] Thomas Zimmermann, [bd] Karl Mandel, [bd] Peter Wasserscheid,[ace] Susanne Wintzheimer *[bd] and Patrick Schühle *[c]

**Liquid organic hydrogen carriers (LOHC) represent a promising technology for future hydrogen storage and transport applications. For operations that require a certain hydrogen release dynamic (*e.g.* with fast load changes) the endothermal dehydrogenation of hydrogen-loaded LOHC compounds can greatly benefit from heating technologies that allow a fast hydrogen release with minimal energy losses. This contribution demonstrates that direct induction heating of the catalyst material represents a very interesting technology in this context as the catalyst material is heated specifically, and thus preheating times and heat losses to the environment can be avoided. In detail, this work highlights the dehydrogenation of perhydro dibenzyltoluene (H18-DBT) using inductively heatable Pt-based catalyst materials prepared in three different ways: a) Pt–alumina on steel beads, b) Pt–alumina on a flat FeCrAl-plate, and c) α-alumina core with a γ-alumina shell that contains spray-dried iron oxide (IO) nanoparticle agglomerates and is impregnated with Pt.**

## Introduction

Liquid organic hydrogen carrier (LOHC) systems such as dibenzyltoluene (H18-DBT) are a promising technology for future energy storage and transportation. These systems consist of fuel-like hydrocarbon compounds that possess the capability to reversibly bind hydrogen, facilitating a secure, practical, and economically viable method for storing and transporting hydrogen within the established fuel infrastructure.

Dibenzyl toluene (H0-DBT)/perhydro-dibenzyl toluene (H18-DBT) represents a highly promising liquid organic hydrogen carrier (LOHC) system, primarily owing to its substantial hydrogen storage capacity (6.2 wt%), widespread technical accessibility, and exceptional compatibility with hydrocarbon-based energy infrastructures.[1] The endothermal nature of the hydrogen release through H18-DBT dehydrogenation necessitates a notably high heat of dehydrogenation (65.4 kJ $mol_{H_2}^{-1}$ under reference conditions) on a high temperature level of above 250 °C.[2] Consequently, effective heat input into the reactor is key to an overall efficient energy storage process. Thus, the optimization of heat provision and integration aspects are essential for the technical application of this LOHC system.[1,3,4]

Current LOHC systems typically rely on continuously operated fixed bed reactors (*i.e.*, catalyst pellets placed in tubes as packed beds) heated *via* a heat transfer fluid. To optimize the energy supply, the coupling of the dehydrogenation process with waste heat from diverse sources, or the design of a hot pressure swing reactor concept has been reported in the literature.[5] Additionally, the combination of different types of fuel cells with a LOHC release unit, the use of burners (porous media burner, free laminar flame) for the direct heating of the dehydrogenation reactor[6] or the development of membrane reactors to achieve dehydrogenation reactions at lower temperatures were studied.[1,7,8] However, all these concepts have in common that they rely on "contact" heating. Therefore, the hydrogen production rate and its cost efficiency highly depend on the feed and wall temperatures of the reactor due to the endothermicity of the reaction and the required heat transfer from the walls to the fluid.[9]

[a] *Helmholtz Institute Erlangen-Nürnberg for Renewable Energy (IEK-11), Forschungszentrum Jülich GmbH, Cauerstraße 1, 91058 Erlangen, Germany*
[b] *Department of Chemistry and Pharmacy, Inorganic Chemistry, Friedrich-Alexander-Universität Erlangen-Nürnberg (FAU), Egerlandstraße 1, 91058 Erlangen, Germany. E-mail: susanne.wintzheimer@fau.de*
[c] *Friedrich-Alexander-Universität Erlangen-Nürnberg (FAU), Lehrstuhl für Chemische Reaktionstechnik (CRT), Egerlandstr. 3, 91058 Erlangen, Germany. E-mail: patrick.schuehle@fau.de*
[d] *Fraunhofer-Institute for Silicate Research ISC, Neunerplatz 2, 97082 Würzburg, Germany*
[e] *Forschungszentrum Jülich GmbH, Institut für nachhaltige Wasserstoffwirtschaft (INW), Am Brainergy Park 4, 52428 Jülich, Germany*

† Electronic supplementary information (ESI) available. See DOI: https://doi.org/10.1039/d4cy00272e

‡ These authors contributed equally to this work.



This journal is © The Royal Society of Chemistry 2024

Open Access Article. Published on 19 July 2024. Downloaded on 8/10/2025 9:45:46 PM.
This article is licensed under a Creative Commons Attribution 3.0 Unported Licence.

In contrast to this, induction heating introduces thermal energy contactless to a chemical reactor and thus, displays an attractive alternative to conventional methods like heat convection, conduction, and/or radiation. Induction heating exploits the electromagnetic properties of a magnetically susceptible material, also called a susceptor. Heat is directly generated in the susceptor exposed to a varying magnetic field that is provided by an alternating current generator.[10] Susceptors require either magnetic or electrically conductive properties to be inducible by the alternating magnetic field. Consequently, either iron oxide, cobalt, or nickel, as well as transition metals, lanthanides, or alloys are the materials of choice.[11] Energy conversion occurs due to hysteresis losses in ferromagnetic susceptors, relaxation losses in superparamagnetic nanoparticles, and eddy currents in electrically conductive samples.

Induction heating has already been demonstrated for numerous endo- and exothermal heterogeneous catalytic reactions (cross-couplings, oxidations, dehydrations, isomerizations, Fischer–Tropsch reactions, dehydrogenations) in batch and flow reactors.[11–17] Through the integration of the susceptor into a heterogeneous catalyst, the inductively produced heat is directly delivered at the catalyst site where it is needed,[14,17] which is superior to simple physical catalyst–susceptor-mixtures.[13]

Classical "contact" heating reactors encounter substantial heat transfer losses, because heat is generally transmitted from an external source over the reactor material and the reaction phase to the catalyst (Fig. 1a). Due to the direct heat generation at the catalyst without appreciable thermal inertia (reactor material, reaction phase), heat transfer losses are avoided by inductive heating.[10,14] Induction heating consequently yields a uniform temperature distribution within the reactor, accelerated reactions, shorter required reaction times to achieve a given value of reactant conversion, and short response times of the reaction enabling on-demand and dynamic product formation.[14,17] Anticipating that induction heating provides a higher temperature on the catalyst surface but simultaneously keeps the temperature of the reaction media and reactor material lower, higher conversions and yields are achievable compared to conventional external heating at the same temperatures of the reaction medium.[12,14] It has been shown that the surface temperature of an inductively heated particle can be significantly higher than the surrounding bulk.[18] This additionally results in reduced heat loss (dissipation phenomena), as well as reduced "heat waste" and thus, often in a reduced formation of by-products and less catalyst fouling problems.[10,14] All in all, contactless heat management in a catalytic reaction based on induction heating can yield optimized dynamics, better process control, setup simplification, safety-enhanced operation, lower operational costs, and enhanced productivity. For endothermal catalytic reactions with a high energy demand, inductive heating promises an improved overall energy balance and dynamic process operation with short response times.[10,11,13–15]

Consequently, direct inductive heating of a dehydrogenation catalyst offers a highly promising approach to reach on-demand hydrogen release from the LOHC system, combined with high energy efficiency. Along these lines, we have developed inductively heatable LOHC dehydrogenation catalysts. Using these materials, the inductively heated

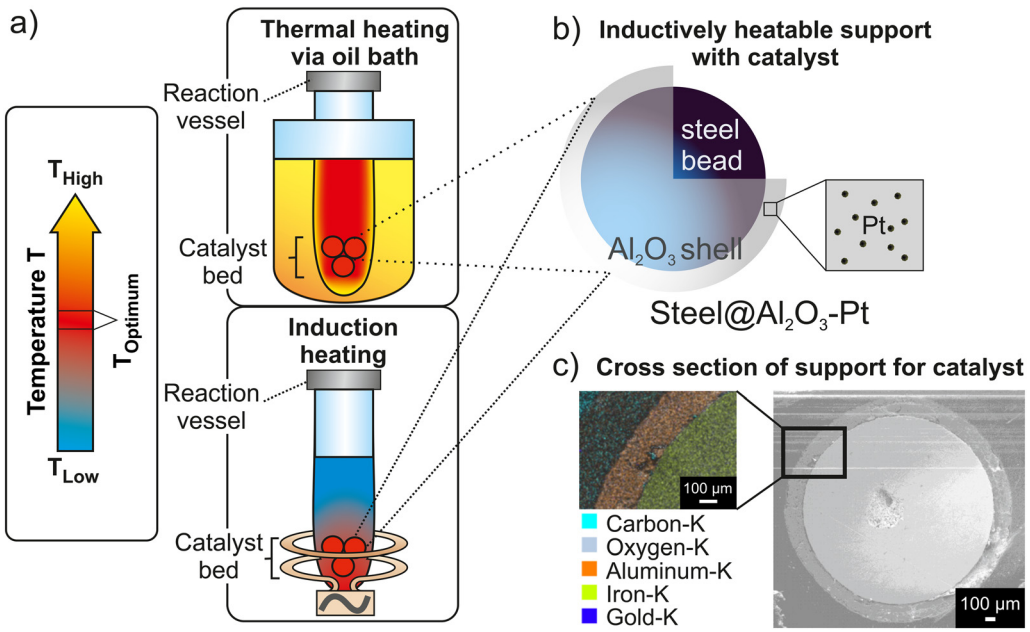


**Fig. 1** a) Scheme of heat input into a fixed-bed reactor *via* inductive (on the bottom) *versus* thermal heating (on the top). b) Scheme of the synthesized *Steel@Al$_2$O$_3$–Pt* catalyst particle consisting of a steel core and an alumina shell impregnated with Pt. c) SEM image of a cross-section of the *Steel@Al$_2$O$_3$–Pt* and its elemental mapping *via* energy-dispersive X-ray spectroscopy.

Open Access Article. Published on 19 July 2024. Downloaded on 8/10/2025 9:45:46 PM.
This article is licensed under a Creative Commons Attribution 3.0 Unported Licence.

dehydrogenation of H18-DBT was studied using a batch reactor (see ESI† for details, Fig. S1) and the obtained results were compared to conventional thermal heating.

## Results and discussion

Following the detailed procedure described in the Experimental section (ESI†), firstly, Pt/alumina eggshell catalysts containing a steel core (fraction of 2.0 to 2.4 mm spheres) and an alumina shell impregnated with Pt were synthesized (Fig. 1b). These materials are denoted as *Steel@$Al_2O_3$–Pt* hereafter. Scanning electron microscopy (SEM) studies of a cross-section of *Steel@$Al_2O_3$–Pt* demonstrated the full coverage of the steel bead by a roughly 170 μm thick alumina shell (Fig. 1c and S2†).The Pt loading of the spray-coated layer was determined to be 2.66 wt% by inductively coupled plasma atomic emission spectroscopy (ICP-AES). The medium composition of the full catalyst bead was 87.82 wt% steel-core, 11.85 wt% $Al_2O_3$ and 0.32 wt% Pt. The catalyst displays pore sizes in the range of 5 to 20 nm (determined *via* nitrogen sorption measurements, Fig. S5†). This pore size range is in good accordance with reported Pt-catalysts for H18-DBT dehydrogenation.[19,20] The inductive heatability of the obtained catalyst beads was evidenced *via* heating curve records (temperature over time, Fig. S6†), placing the solid sample in the center of the inductor coil and applying magnetic fields of 6–300 Oe and frequencies of 1419 kHz. As expected *Steel@$Al_2O_3$–Pt* is heated in the alternating magnetic field due to induced eddy current losses and reaches an equilibrium temperature (induced heat *vs.* heat dissipation to the surrounding) dependent on the applied field strength.

The obtained catalyst *Steel@$Al_2O_3$–Pt* was subsequently tested for the induction heating of the H18-DBT dehydrogenation in a batch reactor as described in the Experimental section (ESI,† including Fig. S1). In Fig. 2a, the continuously monitored temperature of the bulk liquid in the reactor is shown in combination with the measured hydrogen productivity and the resulting degree of dehydrogenation (DoD) over the reaction time.

After the power input was started, the temperature of the bulk increased instantaneously from 25 to 185.3 °C within the first 2.2 min (Fig. 2a bottom graph). Note, that this time can be even shorter if a higher magnetic field is applied and stepwise decreased afterwards. After 2.2 min the hydrogen production started (Fig. 2a top graph inset). As the equilibrium conversion at the measured bulk temperature and atmospheric pressure is below 1%,[21] the catalyst temperature must have already reached significantly higher temperatures compared to the ones measured in the bulk. After 8 min, a temperature of 258.0 °C was reached in the bulk liquid. Afterwards, the temperature increased slowly to 280.2 °C after 87 min reaction time. In the experiment, the maximum hydrogen release was measured soon after the reaction started. Subsequently, a steady almost linear decrease in hydrogen production was observed, while the

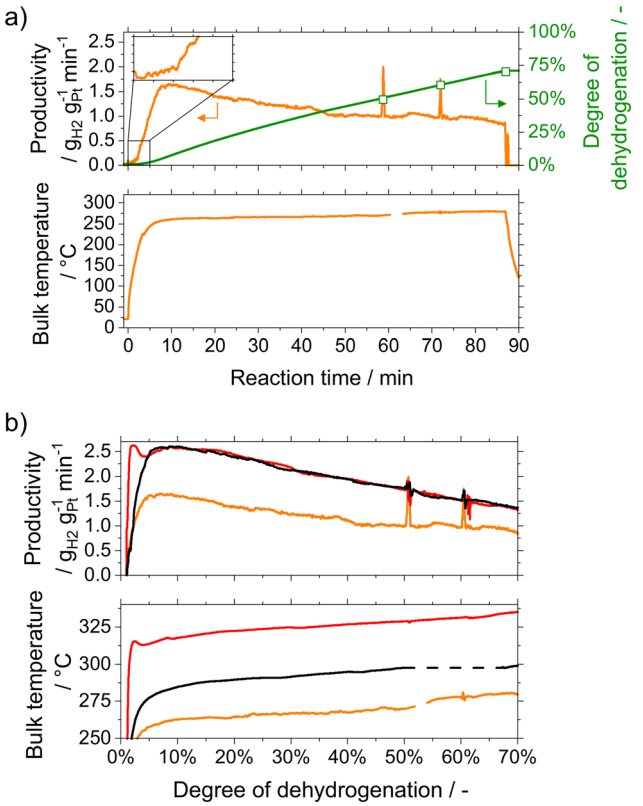


**Fig. 2** a) Productivity, DoD (top graph), and bulk temperature (bottom graph) for the inductively heated batch dehydrogenation of H18-DBT using *Steel@$Al_2O_3$–Pt*. Liquid samples were taken at a DoD of 50%, 60%, and 70% for byproduct analysis and validation of the calculated DoD *via* hydrogen release (□). Reaction conditions: $m_{cat}$ = 280.6 mg, $w_{Pt}$ = 0.32 wt%, $m_{LOHC}:m_{Pt}$ = 2250, $P_{induction\ device}$ = 207 W. b) Productivity (top graph) and bulk temperature (bottom graph) for the dehydrogenation of H18-DBT depending on the DoD in a thermally heated (red) and inductively heated batch experiment with two different power inputs (black, orange) using *Steel@$Al_2O_3$–Pt*. Reaction conditions: $w_{Pt}$ = 0.32 wt%, $m_{LOHC}:m_{Pt}$ = 2250, $m_{cat,red}$ = 285.5 mg, $m_{cat,black}$ = 288.1 mg, $m_{cat,orange}$ = 280.6 mg, induction device settings orange 145 Oe (magnetic field amplitude), induction device settings black 152 Oe (magnetic field amplitude).

DoD asymptotically increased. The lower hydrogen production can be directly related to the DoD as the substrate concentration in the liquid phase decreases with increasing DoD. The correlation between DoD and $H_2$ productivity should follow an exponential decline according to the literature.[22] In our case on the other hand, the steady temperature increase led to the observed linear decline. After 59 min, a DoD of 50% was reached (determined from the accumulated hydrogen release) and a liquid sample was taken. Further liquid samples were taken after 72 min at a DoD of 60% and at the end of the experiment at a DoD of 70%. The liquid samples were analyzed by nuclear magnetic resonance (NMR) and gas chromatography with flame ionisation detector (GC-FID) to validate the degree of dehydrogenation and to determine the byproduct formation (discussed later). We assume, that the decreasing energy consumption by the endothermic dehydrogenation reaction

 This journal is © The Royal Society of Chemistry 2024

Open Access Article. Published on 19 July 2024. Downloaded on 8/10/2025 9:45:46 PM.
This article is licensed under a Creative Commons Attribution 3.0 Unported Licence.

due to a decreasing productivity (*i.e.*, inclining DoD in the batch reaction) results in a steady increase of the catalyst temperature and thus also of the bulk temperature at constant inductive power input (from 8 to 87 min reaction time).

Increasing the power input of the induction device slightly from 145 Oe to 152 Oe led to a strong increase in the productivity to a maximum value from 1.40 to 2.60 $g_{H_2}\ g_{Pt}^{-1}\ min^{-1}$ at a DoD of 8.5% (Fig. 2b top graph, black curve). Here, the bulk temperature increased from 284.6 °C at DoD of 10% to 299.4 °C at DoD of 70% (Fig. 2b bottom graph, black curve) during the experiment. The comparison of the two inductively heated experiments demonstrates, that the hydrogen production rate with the novel *Steel@$Al_2O_3$–Pt* catalysts can be easily adjusted by adapting the power of the induction heater. This enables hydrogen supply from LOHC in a dynamic manner on demand.

A similar dehydrogenation experiment with the catalyst *Steel@$Al_2O_3$–Pt* was conducted using thermal heating (ESI† Fig. S1) in an already pre-heated oil bath. Also in this experiment, the bulk temperature in the reactor was continuously monitored. Note, that the temperature at the active site of the catalyst would be required for a proper comparison of both heating methods. However, this temperature is not easily accessible, in particular because a common thermocouple is a susceptor for inductive heating by itself. Indirectly, the temperature at the catalytic sites can be determined based on the measured hydrogen release productivity. For a given catalyst the productivity depends on the substrate concentration (or DoD) and on the temperature of the active site. Hence, a similar temperature of the active site is achieved if a similar productivity is determined at a similar DoD independent on the heating method. To enable a comparison of both heating methods, the heating bath temperature of the thermally heated reaction was continuously altered to mimic the productivity of the inductively heated catalyst, where the induction device was kept at a constant power input (Fig. S7†). In this way a similar productivity at the respective DoD (continuously controlled *via* a mass flow meter, MFM) could be realized in both experiments.

As expected for batch experiments, a steady decrease of the productivity with increasing DoD (or decreasing substrate concentration) was observed after the start-up phase and after reaching the maximal productivity of 2.60 $g_{H_2}\ g_{Pt}^{-1}\ min^{-1}$ at a DoD of 10% in both cases (Fig. 2b top graph, red and black curves). As a result of the continuous oil bath temperature adjustment, the bulk LOHC temperature of the thermally heated reaction (Fig. 2b bottom graph, red curve) increased continuously from 317.7 °C at a DoD of 10% to 335.6 °C at the final DoD of 70%. Despite similar hydrogen productivities, the bulk temperature was around 35 K higher compared to the temperature of the inductively heated experiment with similar productivity at the respective DoD (temperature increase from 284.6 °C at DoD of 10% to 299.4 °C at DoD of 70%, Fig. 2b bottom graph, black curve). The catalyst temperature is aimed to be similar in both experiments but the temperature gradient to its surrounding must be directed in the opposite direction (inductive heating: catalyst temperature > bulk temperature > reactor wall temperature; thermal heating: reactor wall temperature > bulk temperature > catalyst temperature). Hence, the temperature at the active catalytic sites is in between the bulk temperatures of the inductive and thermal experiment. In a recently published work by Willer *et al.*, the heat transfer in a thermally heated fixed bed reactor was studied in detail for the dehydrogenation of LOHCs. These authors found that the heat transfer in thermally heated systems suffers from a partial to complete coverage of the catalyst by a gas layer consisting of produced hydrogen and evaporated LOHC compounds, and that this reduces the heat transfer to the active site.[23] This resistance layer does not affect the heat transfer using inductive heating. Here, the heat can be effectively transported from the source to the active site through the solid spray-coated layer of γ-alumina (thermal conductivity 35 $W\ m^{-1}\ K^{-1}$ (ref. 24)).

Regarding the byproduct formation (Fig. S8†), a steady increase of the byproduct fraction in the liquid sample with higher DoD can be observed in the experiments with both heating methods. The major by-products are ortho, *meta* and *para* methylfluorenes, which are the deep-dehydrogenation products of the hydrogen release process under investigation. In two experiments showing the same hydrogen productivity (red and black data points), nearly identical byproduct formation (0.47–0.52% at DoD of 70%) was observed, regardless of the heating method, as expected for a similar catalyst temperature.[25] Only the experiment that resulted in a lower hydrogen productivity due to a less intense power input of the induction heater (orange data points) showed a lower byproduct fraction (0.22% at DoD of 70%). This presumably results from a lower catalyst surface temperature. All in all, the inductive heating concept does not change the formation of side products, compared to the conventional heating approach.

Furthermore, the robustness of the material was checked with SEM and ICP-AES measurements of spent *Steel@$Al_2O_3$–Pt* catalysts. Due to the spherical geometry of both the core and spray-coated layer, the difference in thermal expansion coefficient during harsh inductive heating might result in cracks and splintering. However, the SEM images of the catalyst after reaction shown in Fig. S15† do not indicate any damage to the layer, that might have occurred during the inductively heated dehydrogenation experiments. Thus, no damage to the layer was caused during the inductively heated dehydrogenation experiments. The Pt loading of the spent catalyst was determined to be 2.19 wt% by ICP-AES compared to 2.66 wt% of the fresh catalyst (deviation in the range of <±10% of the mean value).

Extremely fast heating ramps and the significant difference in the bulk and catalyst temperatures at the start

Open Access Article. Published on 19 July 2024. Downloaded on 8/10/2025 9:45:46 PM.
This article is licensed under a Creative Commons Attribution 3.0 Unported Licence.

of the catalytic reaction (as described before) are relevant advantages of the use of inductive heating in LOHC dehydrogenation. Recently, Solymosi *et al.* have shown that for heterogeneous catalysts in liquids, rate limitations can occur due to the nucleation of gas bubbles in the pores of the support material if at least one of the products is gaseous.[22] It was shown, that the nucleation–inhibition can be overcome, *e.g.*, by overheating of the catalyst and the nearby liquid. When a thermally heated setup is used for the LOHC dehydrogenation, the whole reaction volume including the bulk liquid has to be overheated to trigger nucleation (temperature gradient from outside to inside, see Fig. 1a). Using inductive heating, however, overheating of the catalyst can be achieved very quickly and efficiently, with minimal thermal stress on the bulk LOHC liquid. Reducing the power input after the catalyst reactivation and bubble formation results in an efficient heat transfer from the catalyst particles to the cooler bulk liquid, allowing the catalyst to cool down to the desired reaction temperature very fast.

Besides spherical catalyst beads in fixed-bed reactors, also plate reactors have been used for the dehydrogenation of LOHC systems.[26,27] Plate reactors offer the advantage of a reduced pressure drop at high volumetric power densities compared to fixed-bed reactors.[26] For demonstrating the transferability of the *Steel@$Al_2O_3$–Pt* (SEM and EDX cross section analysis in Fig. S3†) design from a bead to a plate catalyst, a FeCrAl-plate providing the same alumina–Pt coating (same pore size distribution, Fig. S5†) as *Steel@$Al_2O_3$–Pt* was synthesized (denoted as *Plate@$Al_2O_3$–Pt*) and tested for inductively heated H18-DBT dehydrogenation in comparison to the thermally heated reaction. As expected, the inductive heating performance of *Plate@$Al_2O_3$–Pt* (Fig. S7†), its hydrogen release productivity, and the measured bulk temperature were comparable to the *Steel@$Al_2O_3$–Pt* experiment (Fig. 2 and S9†). Using the plate catalyst, the bulk temperature was 25 to 30 K lower in the inductively heated experiment compared to the thermally heated one at the same hydrogen productivity and DoD. A more detailed discussion is also found in the ESI.† To investigate the stability of these samples, *Plate@$Al_2O_3$–Pt* was recycled for the batch H18-DBT dehydrogenation reaction. The experimental procedure is described in the ESI.† As shown in Fig. S14,† the first run was performed up to a DoDh of 70%. The second run, after recycling the catalyst, showed a similar starting activity up to a DoDh of close to 30% (the experiment had to be stopped out of practical reasons in the laboratory). This very similar course of hydrogen productivity indicates, that no deactivation of the catalyst happened in the first run and the material can be considered stable. More tests on the

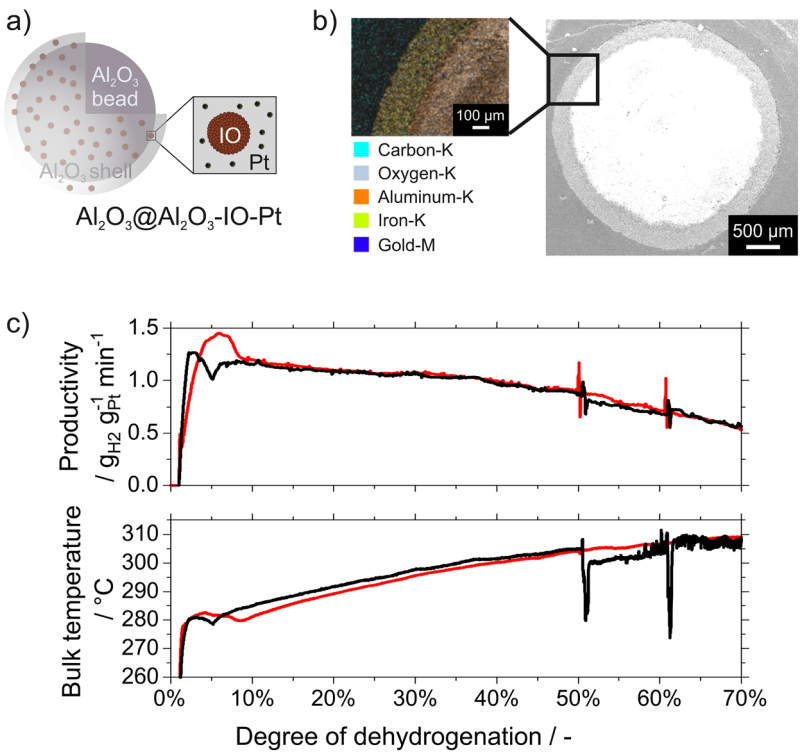


**Fig. 3** a) Scheme of the synthesized *$Al_2O_3$@$Al_2O_3$–IO–Pt* catalyst particle consisting of an alumina core and an alumina shell that contains IO supraparticles and is impregnated with Pt. b) SEM image of a cross-section of *$Al_2O_3$@$Al_2O_3$–IO–Pt* and its elemental mapping. c) Productivity (top graph) and bulk temperature (bottom graph) for the dehydrogenation of H18-DBT depending on the DoD in a thermally heated (red) and inductively heated (black) batch experiment using *$Al_2O_3$@$Al_2O_3$–IO–Pt* as the catalyst. Reaction conditions: $w_{Pt}$ = 0.24 wt%, $m_{LOHC}:m_{Pt}$ = 1900, $m_{cat,red}$ = 430.0 mg, $m_{cat,black}$ = 429.0 mg, induction device settings: 273 Oe.

 This journal is © The Royal Society of Chemistry 2024

Open Access Article. Published on 19 July 2024. Downloaded on 8/10/2025 9:45:46 PM.
This article is licensed under a Creative Commons Attribution 3.0 Unported Licence.

recyclability or long-term stability of our catalyst will be the subject of our future work.

In this study, a further approach was followed to reach inductively heatable LOHC dehydrogenation catalysts. Besides using coated steel beads or FeCrAl-plates as susceptors, inductively heatable nanoparticles were incorporated into a rather conventional $Al_2O_3$-supported catalyst. For this approach, a Pt/alumina eggshell catalyst consisting of an α-alumina core and a γ-alumina shell containing spray-dried iron oxide (IO) nanoparticle agglomerates, also called IO supraparticles, was impregnated with Pt, and denoted as *$Al_2O_3$@$Al_2O_3$–IO–Pt* (Fig. 3a). In this catalyst design, the total catalyst weight could be significantly decreased compared to *Steel@$Al_2O_3$–Pt* with dense steel cores. The roughly 200 μm thick alumina shell containing 1–20 μm sized IO supraparticles is visible in scanning electron microscopy (SEM) studies of a cross-section of *$Al_2O_3$@$Al_2O_3$–IO–Pt* (Fig. 3b and S4†). The Pt loading per catalyst was determined to be 0.24 wt% by ICP-AES. The Fe-loading was determined to be 9.21 wt% equaling a weight load of 11.7 wt% IOs. The catalyst displays pore sizes in the range of 5 to 20 nm as well as larger pores and an overall higher pore volume compared to *Steel@$Al_2O_3$–Pt* (determined *via* nitrogen sorption measurements, Fig. S5†). The modified pore structure and volume are caused by the introduction of IO supraparticles and their intra-supraparticle pores within the porous alumina coating. *$Al_2O_3$@$Al_2O_3$–IO–Pt* nevertheless provides the intended accessibility of the active Pt sites for the 18H-DBT in the dehydrogenation reaction. The IO-induced inductive heatability of the obtained catalyst is evidenced by the heating curve records (temperature over time) shown in Fig. S6.† In such ferromagnetic materials the inductive effect predominantly results from the mechanism of hysteresis loss heating, while eddy currents are responsible for the inductive heatability of the previously discussed steel bead catalysts. The benefit of hysteresis loss heating is, that this effect only appears below the so-called Curie-temperature of a material.[10] Above this temperature, the material loses its ferromagnetic characteristics. Thus, the maximal temperature of a catalyst can be adjusted by tuning the Curie temperature[10] which will be a particular focus of our future studies. Due to the occurring hysteresis losses, the novel *$Al_2O_3$@$Al_2O_3$–IO–Pt* catalyst has been heated in an alternating magnetic field. However, compared to the *Steel@$Al_2O_3$–Pt* catalyst higher field strengths are required to achieve temperatures suitable for LOHC dehydrogenation because of the significantly reduced amount of inductively heatable material in the reactor. In addition, the coercive field strength of the inductively heatable material must be overcome to magnetize the sample and trigger hysteresis loss.[28] While applying an alternating magnetic field of 273 Oe, the sample reached an equilibrium temperature, probably due to heat dissipation to the surroundings.

Fig. 3c shows the productivity and the measured bulk temperature plotted over the DoD in the thermally and inductively heated H18-DBT dehydrogenation experiment (respective plots over the reaction time are displayed in Fig. S10 and S11†). Once again, the temperature of the thermally heated reaction was adjusted to mimic the productivity obtained by a constant power input in the inductively heated experiment.

At a DoD of 10%, the obtained maximum productivity was 1.16 $g_{H_2}$ $g_{Pt}^{-1}$ $min^{-1}$ and decreased continuously to 0.59 $g_{H_2}$ $g_{Pt}^{-1}$ $min^{-1}$ at a final DoD of 70%. Similar to *Steel@$Al_2O_3$–Pt*, the temperature steadily increased from a DoD of 10% to the final DoD of 70% from 281 °C to 310 °C using thermal heating and from 285 °C to 309 °C using inductive heating. During the experimental run, we could observe a heating of the common thermocouple itself as mentioned before. An immediate temperature drop of up to 9.5 K was measured when the induction device was switched off (see Fig. S12†). This was not observed in the previous experiments, probably due to the lower power of the magnetic field that was required to reach the desired reaction temperature of around 300 °C. Hence the measured bulk temperature again is expected to be lower than the bulk temperature in the thermally heated experiment but not as pronounced. Because a higher power input to inductively heat *$Al_2O_3$@$Al_2O_3$–IO–Pt* was required while a significantly lower amount of hydrogen was released, it seems plausible that a higher share of the introduced energy is used to heat the bulk phase resulting in a higher bulk temperature and thus, a lower temperature difference between bulk and catalyst temperature. The inclining temperatures changed the expected exponential productivity decrease as already discussed for *Steel@$Al_2O_3$–Pt*. However, contrary to the previously shown data, no linear decrease in productivity nor a linear increase in the temperatures was observed for *$Al_2O_3$@$Al_2O_3$–IO–Pt*. While the temperature increased asymptotically, productivity barely decreased by only 10% up to a DoD of 35% and more strongly afterward. Due to similar productivities, induced by similar catalyst temperatures, the byproduct formation was nearly identical in both heating methods (Fig. S13†).

A thorough comparison in terms of productivity, costs, and stability of the inductively heatable catalysts and technologies with conventional approaches is difficult in this early stage, as it is influenced by a multitude of aspects. However, more general aspects are compared in the following, and the potential of inductively heatable approaches for LOHC dehydrogenation is discussed. Our experimental investigations show, that the inductively heated catalyst materials have the potential to perform at least similar to standard H18-DBT dehydrogenation catalysts when compared under identical platinum contents. In the example of the *Steel@$Al_2O_3$–Pt* catalysts, this is because the composition of the catalytic layer is identical to conventional catalysts, with the only difference, that this porous layer is not deposited on an $Al_2O_3$ core (conventional egg–shell catalyst) but on an inductively heatable steel bead. However, the degree of utilization of the platinum in an inductively heated reactor has the potential to be significantly higher, as the required temperature is achieved directly by applying

Open Access Article. Published on 19 July 2024. Downloaded on 8/10/2025 9:45:46 PM.
This article is licensed under a Creative Commons Attribution 3.0 Unported Licence.

heat to the catalyst. This could lead to a more homogeneous temperature field in the reactor in the future and thus to an overall better performance of the $H_2$ release. The total costs of the LOHC dehydrogenation step result from a large number of individual aspects, such as the catalyst costs, the size of the apparatus and reactor, and the energy required for heating. When comparing conventional and inductively heatable catalysts, there are only minor cost differences, as the additional catalyst components for inductive heating, such as steel and iron oxide, are inexpensive and therefore of minor significance. The energy costs are influenced by the relationship between future heat (conventional heating) and electricity costs (inductive heating) and their availability, as well as by the energy efficiency of inductive heating. Here, the materials coated on steel spheres could have advantages over materials impregnated with IO nanoparticles, as these are heated *via* the more energy-efficient mechanism of eddy current instead of hysteresis-loss heating. On the other hand, the heated catalyst mass is lower with the IO nanoparticle-based materials. Regarding stability, no degradation of the *Steel@$Al_2O_3$–Pt* catalysts and no decrease in activity in the recycle of the *Plate@$Al_2O_3$–Pt* catalysts could be observed in our experiments. However, a stability study under continuous operating conditions is still pending. A more homogeneous temperature distribution on the inductively heated catalysts offers the potential for lower by-product or coke formation as in conventional heating. On the other hand, the fast and dynamic response time of the inductive heater may increase the risk of physical stress and overheating of the catalyst during long-term operation.

## Conclusion

Three types of Pt–alumina catalysts with inductive heating properties were developed and applied for the inductively heated dehydrogenation of the LOHC compound H18-DBT. In the first and second approach an electrically conductive core material (spherical and flat) was coated by an active Pt–alumina layer, while the third approach included the deposition of ferromagnetic nanoparticles on an alumina/Pt pellet catalyst. Inductive heating was shown to allow for a very fast heating ramp and thus very dynamic hydrogen release without any negative effects on the by-product formation in H18-DBT dehydrogenation. As only the catalyst is heated, and not the reactor material and reaction mixture, inductive heating is a promising technology to reduce heat losses to the environment and to increase the dynamics of on-demand hydrogen release, as required in many applications of the future hydrogen economy.

## Data availability

Data for this article are available at Zenodo at **https://doi.org/10.5281/zenodo.12650754**.

## Author contributions

Conceptualization: M. S., T. S., T. R., T. Z., K. M., P. W., S. W., and P. S. Methodology: M. S., T. S., T. R., P. N., T. Z., S. W., and P. S. Investigation: M. S., T. S., T. R., P. N., N. P. J., T. Z. Visualization: M. S., T. S., T. R., S. W., and P. S. Funding acquisition: S. W. and P. S. Project administration: M. S., T. S., T. R., S. W., and P. S. Supervision: M. S., T. S., T. R., S. W., and P. S. Writing (original draft): M. S., T. S., T. R., S. W., and P. S. Writing (review & editing): all authors.

## Conflicts of interest

P. W. is a founder and a minority shareholder of the company Hydrogenious LOHC Technologies (**https://www.hydrogenious.net**) that offers commercial hydrogen storage systems based on the LOHC technology. Further conflicts of interest are not to declare.

## Acknowledgements

This work was financially supported by the Klaus Tschira Boost Fund (KT44), a joint initiative of the German Scholars Organization and the Klaus Tschira Stiftung, and by the Deutsche Forschungsgemeinschaft (DFG, German Research Foundation, SFB 1452), which are gratefully acknowledged. Furthermore, the authors thank the German Federal Ministry for Economic Affairs and Climate Action for funding this work (LOReley project, 03E13023A-F). The authors thank BÜCHI Labortechnik GmbH for providing the spray-dryer equipment.

## References

1 J. Bollmann, K. Mitländer, D. Beck, P. Schühle, F. Bauer, L. Zigan, P. Wasserscheid and S. Will, *Int. J. Hydrogen Energy*, 2023, **48**, 30039–30056.
2 K. Müller, K. Stark, V. N. Emel'yanenko, M. A. Varfolomeev, D. H. Zaitsau, E. Shoifet, C. Schick, S. P. Verevkin and W. Arlt, *Ind. Eng. Chem. Res.*, 2015, **54**, 7967–7976.
3 C.-I. Ahn, Y. Kwak, A.-R. Kim, M. Jang, A. Badakhsh, J. Cha, Y. Kim, Y. S. Jo, H. Jeong, S. H. Choi, S. W. Nam, C. W. Yoon and H. Sohn, *Appl. Catal., B*, 2022, **307**, 121169.
4 Y. Jo, J. Oh, D. Kim, J. H. Park, J. H. Baik and Y.-W. Suh, *Korean J. Chem. Eng.*, 2022, **39**, 20–37.
5 H. Jorschick, P. Preuster, S. Dürr, A. Seidel, K. Müller, A. Bösmann and P. Wasserscheid, *Energy Environ. Sci.*, 2017, **10**, 1652–1659.
6 P. Preuster, Q. Fang, R. Peters, R. Deja, V. N. Nguyen, L. Blum, D. Stolten and P. Wasserscheid, *Int. J. Hydrogen Energy*, 2018, **43**, 1758–1768.
7 K. Müller, T. Skeledzic and P. Wasserscheid, *Energy Fuels*, 2021, **35**, 10929–10936.
8 Y. Sekine and T. Higo, *Top. Catal.*, 2021, **64**, 470–480.
9 N. Rao, A. K. Lele and A. W. Patwardhan, *Int. J. Hydrogen Energy*, 2022, **47**, 28530–28547.

 This journal is © The Royal Society of Chemistry 2024

Open Access Article. Published on 19 July 2024. Downloaded on 8/10/2025 9:45:46 PM.
This article is licensed under a Creative Commons Attribution 3.0 Unported Licence.

10 W. Wang, G. Tuci, C. Duong-Viet, Y. Liu, A. Rossin, L. Luconi, J.-M. Nhut, L. Nguyen-Dinh, C. Pham-Huu and G. Giambastiani, *ACS Catal.*, 2019, **9**, 7921–7935.
11 S. Ceylan, C. Friese, C. Lammel, K. Mazac and A. Kirschning, *Angew. Chem., Int. Ed.*, 2008, **47**, 8950–8953.
12 S. R. Chaudhuri, J. Hartwig, L. Kupracz, T. Kodanek, J. Wegner and A. Kirschning, *Adv. Synth. Catal.*, 2014, **356**, 3530–3538.
13 J. Garcia-Aguilar, J. Fernandez-Garcia, E. V. Rebrov, M. R. Lees, P. Gao, D. Cazorla-Amoros and A. Berenguer-Murcia, *Chem. Commun.*, 2017, **53**, 4262–4265.
14 C. Huang, Y. Wang, R. Zhong, Z. Sun, Y. Deng and L. Duan, *Chin. Chem. Lett.*, 2023, **34**, 108101.
15 J. Lee, S. Ga, D. Lim, S. Lee, H. Cho and J. Kim, *Chem. Eng. J.*, 2023, **457**, 141203.
16 A. Meffre, B. Mehdaoui, V. Connord, J. Carrey, P. F. Fazzini, S. Lachaize, M. Respaud and B. Chaudret, *Nano Lett.*, 2015, **15**, 3241–3248.
17 A. Zadražil and F. Štěpánek, *Chem. Eng. Sci.*, 2015, **134**, 721–726.
18 N. da Silva Moura, K. R. Bajgiran, A. T. Melvin, K. M. Dooley and J. A. Dorman, *ACS Appl. Nano Mater.*, 2021, **4**, 13778–13787.
19 F. Auer, D. Blaumeiser, T. Bauer, A. Bösmann, N. Szesni, J. Libuda and P. Wasserscheid, *Catal. Sci. Technol.*, 2019, **9**, 3537–3547.
20 P. Modisha, P. Gqogqa, R. Garidzirai, C. N. M. Ouma and D. Bessarabov, *Int. J. Hydrogen Energy*, 2019, **44**, 21926–21935.
21 S. Dürr, S. Zilm, M. Geißelbrecht, K. Müller, P. Preuster, A. Bösmann and P. Wasserscheid, *Int. J. Hydrogen Energy*, 2021, **46**, 32583–32594.
22 T. Solymosi, M. Geisselbrecht, S. Mayer, M. Auer, P. Leicht, M. Terlinden, P. Malgaretti, A. Bosmann, P. Preuster, J. Harting, M. Thommes, N. Vogel and P. Wasserscheid, *Sci. Adv.*, 2022, **8**, eade3262.
23 M. Willer, P. Preuster, M. Geißelbrecht and P. Wasserscheid, *Int. J. Hydrogen Energy*, 2024, **57**, 1513–1523.
24 M. Vasheghani, E. Marzbanrad, C. Zamani, M. Aminy, B. Raissi, T. Ebadzadeh and H. Barzegar-Bafrooei, *Heat Mass Transfer*, 2011, **47**, 1401–1405.
25 P. Modisha and D. Bessarabov, *Sustainable Energy Fuels*, 2020, **4**, 4662–4670.
26 P. Nathrath, Y. Raed Ramzi, M. Bierling, S. Thiele, P. Wasserscheid and P. Schühle, *Catal. Sci. Technol.*, 2024, **14**, 980–989.
27 T. Solymosi, F. Auer, S. Dürr, P. Preuster and P. Wasserscheid, *Int. J. Hydrogen Energy*, 2021, **46**, 34797–34806.
28 V. V. Mody, A. Singh and B. Wesley, *Eur. J. Nanomed.*, 2013, **5**, 11–21.